

Search for gravitational wave trains with the spacecraft ULYSSES

B. Bertotti¹, R. Ambrosini², J. W. Armstrong³, S. Asmar³, G. Comoretto⁴, G. Giampieri^{1*}, I. Iess⁵, Y. Koyama⁷, A. Messeri^{6**}, A. Vecchio¹, and H. D. Wahlquist³

¹Dipartimento di Fisica Nucleare e Teorica, Università di Pavia, I-27100 Pavia, Italy

²Istituto di Radioastronomia, I-40126 Bologna, Italy

³Jet Propulsion Laboratory, California Institute Of Technology, Pasadena, California 91109, USA.

⁴Osservatorio Astrofisico di Arcetri, I-50125 Firenze, Italy

⁵Dipartimento di Ingegneria Aerospaziale, Università di Roma 'La Sapienza', I-00158 Roma, Italy

⁶Istituto di Fisica dello Spazio Interplanetario, I-00044 Frascati, Italy

⁷Kashima Space Research Center, Communications Research Laboratory, Kashima, 314 Japan

Received ; accepted

Abstract. We report on the search for periodic gravitational wave in the mHz band conducted with the spacecraft ULYSSES. Gravitational wave signals generally provide information about the distance of the source; ULYSSES' data have a "km" for each kind of source one looks for; for binaries the galactic centre is accessible to our experiment. The Neyman Pearson method, with its two strategies of 'attempting detection' and getting a threshold for no detection, is discussed with great care. We did not find significant evidence for positive detection, but established, at the 90% confidence level, upper limits to the amplitude significantly better than previous work. The weaker condition $\text{SNR} = 1$ corresponds to signal amplitudes h which vary about from 3×10^{-15} to 10^{-15} from low to high frequencies. Similar results and thresholds have been obtained for chirped signals in the linear regime. We have discussed these limits in relation to a possible, conventional binary system of black holes in the galactic centre as a source. We found that in the plane of the frequency and its rate of increase the corresponding region of significance is small; there we establish for a hypothetical companion of a central black hole of $2106 M_\odot$ the upper limit of $\approx 5800 M_\odot$.

Key words: Gravitation - Galaxies: nuclei

1. Introduction

The space probe ULYSSES has been continuously tracked in a Doppler mode for 28 days from February 20 to March 18, 1992. In addition, 23 passes (including 3.5 days of continuous tracking) are available from the another measurement set about the first solar opposition; however, at that time the round-trip light-time T , about 600 sec, implied a low frequency cut off seven times larger and less interesting data. A description of the experimental setup is given in (Bertotti et al. 1992), where earlier references are given about the Doppler method; a preliminary report is found in (Iess 1994). Generally speaking, the quality of the data, as described by their Allan deviation $\sigma_y(\tau)$, was generally worse than the nominal target, for the experiment ($\sigma_y = 3 \times 10^{-4}$ at an integration time $\tau = 1000$ sec); in particular, data taken at the end of the observation period and near the opposition (at which important manoeuvres affected the spacecraft dynamics and disturbed the Doppler observable) were noisier and have not been used in the present analysis, based upon data of 14 days, from day GO to 74 (see Fig. 1).

An important and new asset of our experiment was the use of two different down-link carriers, in S-band ($\nu_{1S} \approx 2.293$ GHz) and X-band ($\nu_1 \approx 8.408$ GHz); the up-link carrier was instead at a single, S-band frequency ($\nu_1 \approx 2.112$ GHz) and dominated the plasma noise (for a study of multi-frequency links, see Bertotti et al. 1993.) Moreover, for more than 2/3 of the time, a (VLBI) receiving station, in Italy or Japan, in addition to those of the Deep Space Network (DSN) of NASA, was used; the comparison and the correlation between these four, partially independent, time series have been very important in understanding and reducing the noise (see Iess et al. 1987).

Send offprint requests to: B. Bertotti.

Present address: Jet Propulsion Laboratory, California Institute of Technology, Pasadena, California, USA.

Present address: European Space Research Institute, I-00014 Frascati, Italy.

A nother Doppler experiment involving, besides ULYSSES, GALILEO and MARS OBSERVER (which used an X-band carrier both up- and down-link), was carried out for 21 days in March 1993.

While ordinary binary stars have a frequency below our band, cut off at approximately the reciprocal of the round-trip light-time $T \approx 4400$ sec, in a scenario of generalized merging of galaxies, if the parent systems contain in their cores massive black holes, their binding could produce important trains of gravitational waves. The Doppler response to such a class of sources has been discussed in Wahlquist (1987); a search in the range 30 to 2000 sec conducted with the Pioneer 11 data (Armstrong et al. 1987) has set a 90% confidence upper limit at the dimensionless amplitude of 610-14. Anderson et al. (1993), using PIONEER 10 data set up an upper limit of 710-15 for a detection at SNR = 1

similar to a coincidence experiment and has allowed rejection and understanding of troublesome outliers.

The emission of gravitational waves by a binary near the coalescence phase produces a characteristic increase in its frequency ("chirping"), with a well defined law; the technique to extract this special signal from the noise have been discussed and applied to real data by Tinto & Armstrong (1991) and Anderson et al. (1993) in the case in which the acceleration of the frequency may be neglected. In the present paper we have used it, too (Sec. 6); its statistical foundations are discussed in two appendices.

The problem of the construction of adequate filters to detect coalescing binaries has been discussed in several recent papers in connection with the future interferometric detectors (Sathyaprakash & Dhurandar 1991, Dhurandar & Sathyaprakash 1994, Dhurandar et al. 1991, Blanchet & Sathyaprakash 1994, Kokkotas et al. 1993). Most of them deal with the exact expression of the change in frequency and amplitude; our work has the advantage of dealing with real data.

2. The ken⁸ of ULYSSES

Wide band observations of gravitational waves generally provide information about the distance of the source. Collapses emit at the characteristic frequency

$$f = \frac{k_1}{M} \quad (1)$$

and produce at a distance r an amplitude

$$h = \sqrt{\epsilon} \frac{M}{r}. \quad (2)$$

Here ϵ is the efficiency with which rest energy is radiated away; this quantity is uncertain, but should lie between 0.001 and 0.01. Masses are measured in seconds: a solar mass is 4.8 μ sec. For an axially symmetric collapse Piran & Stark (1986, p. 64) have estimated the constant k_1 between 0.035 and 0.08. The frequency of observation determines (with $k_1 \approx 0.06$) the collapsing mass

$$M = \frac{1.3104 \text{ Hz}}{f} M_{\odot} = 1.3104 \frac{\text{mHz}}{(f)} M_{\odot}; \quad (3)$$

the amplitude then determines the distance

$$r = 7 \sqrt{\epsilon} \left(\frac{\text{mHz}}{f} \right) \left(\frac{10^{-13}}{h} \right) \text{ Mpc}. \quad (4)$$

The Virgo cluster is at 20 Mpc.

For periodic sources we have a standard model for the emission of gravitational trains in which the energy loss, excluding other losses, like friction with a medium, is proportional to the square of the third derivative of

Fig. 1. The daily Allan deviation $\sigma_a 10^{14}$ at an integration time $\tau = 1000$ sec for the DSN (squares) and the VL BI data (plus signs); opposition occurred on day 58. The enhancement in the last 4 days was probably due to the interplanetary plasma.

In the present paper particular care is devoted to statistically rigorous criteria to decide about our results. We wish to avoid two errors: false alarm and false dismissal; in an experiment like ours, in which the probability of success is low, we consider the former as primary. Following the Neyman-Pearson theory, we construct in the space X of the observable quantities (for periodic signals, the squares of the spectral amplitudes of the Doppler record) a subset X_1 corresponding to announcement of detection (with a given false alarm probability α); this set should be chosen in such a way as to minimize the false dismissal probability. If the record is not contained in X_1 , for any given gravitational wave amplitude h , we construct another set $X'_0(h)$ corresponding to no detection and increase h until the data point lies on its boundary. This determines an upper limit to the amplitude, with a given level of confidence. The use of different (up to four) different Doppler records although not quite independent - makes our experiment

⁸ From the Oxford Dictionary: 'range of sight or knowledge'.

the quadruple moment. In this case the orbit soon becomes circular and we have a wave train of increasing frequency, amplitude and bandwidth, until final coalescence occurs at, say, $t = t_0$. It must be noted, however, that in presence of friction the eccentricity may increase, rather than decrease, giving a signal of entirely different form (Ebisuzaki et al. 1991; Fukushige & Ebisuzaki 1992; Vecchio et al. 1994 and other papers.) The presence of a dipole contribution in the emission of gravitational waves (e.g., due to a radiating "fifth force") would also give a different signal (Bertotti & Sivaram 1990).

For a strictly periodic signal the Doppler observable $y = \Delta\nu/\nu$ is determined by the dimensionless amplitude $h_1 \equiv h_{\mu\nu}n^\mu n^\nu$ constructed with the null four-vector n^μ along the ray and is given by the real part of

$$y = F(fT, \theta)h_1, \quad (5)$$

where $T = 21$, is the round-trip light-time. The instrumental factor

$$F = \frac{1 - \cos\theta}{2} + \cos\theta e^{-\pi i(1+\cos\theta)fT} - \frac{1 + \cos\theta - 2\pi ifT}{2}$$

generally of order unity, satisfies $0 \leq |F| \leq 2$; it goes to zero when $fT \rightarrow 0$ and also when θ , the angle between the source and the spacecraft, tends to 0 or π . The first limit is required by the Equivalence Principle, the second by the transversal character of gravitational waves (which, by the way, has never been tested). In the form

$$F = \left(e^{-\pi i(1+\cos\theta)fT} - 1 \right) \cos\theta + \\ + \left(e^{-2\pi ifT} - 1 \right) \frac{1 + \cos\theta}{2} \quad (6)$$

the two limiting behaviours are apparent: when $fT \ll 1$

$$F(fT, 0) = \pi ifT(1 - \cos^2\theta) + O(fT)^2;$$

when $\cos\theta = \pm(1 + \delta)$

$$F(fT, \theta) = \left[\delta - \frac{1 - \cos\theta}{2} - \pi ifT \right] + O(62).$$

In the conventional view the emission of gravitational wave by a binary with total mass M and reduced mass μ depends on the *mass parameter*

$$m = \mu^{3/5} M^{2/5}, \quad (7)$$

which appears both in the amplitude

$$h = \frac{\sqrt{35}}{2} \frac{m^{5/3}}{r} [\pi f(t)]^{2/3} \quad (8)$$

and in the frequency

$$\pi f(t) = \frac{5}{(256)}^{3/8} \frac{1}{m^{5/8}(t_0 - t)^{3/8}} \quad (9)$$

The time to coalescence $t_0 - t$ and the frequency determine the mass parameter.

The factor $\sqrt{35}/2$ in h results from averaging h_1^2 over the (unknown) polarization angle φ and the (unknown) angle ι between the normal to the orbital plane and the direction from the source to the observer; they appear in h_1 in the combination

$$2(1 + \cos^2\iota) \cos 2\varphi + 4 \cos\iota \sin 2\varphi.$$

The time to coalescence is related to the distance by

$$\frac{1}{t_0 - t} = \frac{512\pi^2}{2\sqrt{35}} h r f^2 = A h r f^2 \quad (10)$$

The number

$$A = \frac{512\pi^2}{2\sqrt{35}}$$

is about 427.

A Doppler record can be analyzed in *four* different ways, corresponding to decreasing time to coalescence and increasing distance: in going down the list we do increase our ken, but at the expense of looking for sources of shorter lifetime.

- At small distances we can search for a strictly sinusoidal signal; for a record of length T_1 (with the origin of time in the middle) and a frequency resolution $\Delta f = 1/T_1$ this requires

$$\frac{T_1}{2} \frac{df}{dt} = \frac{3}{16} \frac{T_1 f}{t_0 - t} < \frac{1}{T_1}. \quad (11)$$

or

$$\frac{1}{t_0 - t} = A h r f^2 < \frac{16}{3} \frac{1}{f T_1^2}. \quad (12)$$

Taking for reference typical ULYSSES' values, this implies

$$r < \frac{16}{3A} \frac{1}{h T_1^2 f^3} = \\ = 70 \text{ pc} \left(\frac{5 \cdot 10^{-15}}{h} \right) \left(\frac{10^6 \text{ sec}}{T_1} \right)^2 \left(\frac{\text{MHz}}{f} \right)^3 = r_1.$$

The galactic centre is marginally reached at low frequencies.

- We can extend our ken by looking for a linearly chirped signal, characterized by the parameter

$$\beta = \frac{df}{dt}; \quad (14)$$

it must fulfil

$$\frac{T_1^2}{8} \frac{d\beta}{dt} = \frac{T_1^2}{8} \frac{d^2f}{dt^2} = \frac{T_1^2}{8} \frac{33}{64} \frac{f}{(t_0 - t)^2} < \frac{1}{T_1}, \quad (15)$$

that is to say,

$$\frac{1}{t_0 - t} < \frac{16}{3} \frac{1}{f T_1^2} 3 \sqrt{\frac{2}{33}} \sqrt{f T_1}. \quad (16)$$

The previous ken r_1 is now extended to

$$r < 3 \sqrt{\frac{2}{33}} \sqrt{f T_1} r_1 = \\ = 23 r_1 \left(\frac{f T_1}{\text{MHz} \cdot 10^6 \text{ sec}} \right)^{1/2}. \quad (17)$$

3 If

$$\frac{1}{t_0 - t} < \frac{1}{T_1} = \frac{16}{3} \frac{1}{f T_1^2} \frac{3}{16} f T_1 \quad (18)$$

we can search the whole record for the chirped signal with the appropriate, non linear law. In this case the k_{en} is still larger:

$$r < \frac{3}{16} f T_1 \quad r_1 \approx 190 \quad r_1 = \frac{f T_1}{(\text{mHz } 10^6 \text{ sec})} \quad (19)$$

- 4 To reach greater distance we must use even shorter trains, in which coalescence itself is included in the record; this class of sources merges with the wide band pulses. The pulse search with ULYSSES' data will be discussed in another paper.

3. Criteria for detection

We review now the detection criteria for periodic signals (see, e. g., Tinto & Armstrong 1991); the problem of detection with two or more correlated records will be discussed in a separate paper.

A strictly periodic binary system produces a peak in the spectrum $S_y(f)$ of the Doppler observable at twice the orbital frequency (and its harmonics if the eccentricity does not vanish). A search for such peaks with a record of length T_1 is based upon a discrete realization $S_y(f_k)$ of the spectrum, at frequencies f_k spaced by $1/T_1$. We assume that the amplitudes of the spectral noise are gaussian and uncorrelated, with variance $\langle S_y(f_k) \rangle$. The gaussian character is expected on the basis of the Central Limit Theorem: the amplitudes are linear combinations of a large number of random variables, the Doppler record itself.

The normalized spectrum

$$x_k = \frac{S_y(f_k)}{\langle S_y(f_k) \rangle} \quad (20)$$

defines our sample space $X = \{x_k\}$ (restricted to non negative values), with N dimensions. In ULYSSES' record under consideration $N \approx 65,000$, in practice, since a single record is available, the average spectrum $\langle S_y(f_k) \rangle$ is approximated with the average over the band around f_k where the spectrum is approximately constant; indicating with a prime this summation and with N' the number of such terms, we shall deal with

$$x_k = \frac{S_y(f_k)}{\frac{1}{N'} \sum_j' S_y(f_j)} = \frac{S_y(f_k)}{\sigma^2} \quad (21)$$

σ^2 is the mean spectral amplitude, slowly varying with frequency. Similarly, the amplitude Fh of a sinusoidal signal corresponds to a normalized spectral peak

$$|c|^2 + \frac{|Fh|^2}{\sigma^2} \quad (22)$$

Our procedure (see, e.g., Silvey 1970) aims at avoiding two different errors: a) falsely declaring detection and

b) falsely dismissing detection. We proceed in two steps, First we undertake to determine whether we are allowed to declare detection (option A); in this case we give priority to avoiding error a). If this does not succeed, we look for the conditions under which we are allowed to declare no detection and thereby set up an upper limit to h (option B)); in this case the error b) is primary.

With the assumption that the noise is purely random and white, the observable x_k has the simple probability distribution

$$p_0(x_k) = \exp \left(- \sum_k x_k \right) = \prod_k P_0(x_k), \quad (23)$$

with volume element

$$d^N x = \prod_k dx_k$$

We have indicated with

$$P_0(x) = k^{-x} \quad (24)$$

the probability distribution for a single bin. In the real case the assumption of a flat spectrum is not quite correct, but this assumption can be tested with the data (see Fig. 3). Neglecting the (small) correlation between different spectral bins decreases the probability of false alarm; however, since we shall declare no detection, this has the effect of making our threshold somewhat higher than necessary.

In option A) we shall announce detection if one or more of the coordinates is larger than a threshold \bar{x} , to wit, if x_k lies outside the cube $C_{\bar{x}}$ of side \bar{x} . This threshold is determined by the requirement that the false detection probability is c_k , that is to say,

$$1 - \int_{C_{\bar{x}}} d^N x p_0(x_k) = 1 - (1 - e^{-\bar{x}})^N = \alpha. \quad (25)$$

Since $\alpha \ll 1$ this is approximated by

$$N e^{-\bar{x}} = \alpha + \frac{1}{2} \alpha^2 + \dots \quad (26)$$

In ULYSSES' case, with $N = 65,000$ and $\alpha = 0.1$, $\bar{x} = 13.38$.

In option B) we introduce in X the probability measure $p_h(x_k)$ when a signal of amplitude Fh and random phase is added to the gaussian noise; for a single frequency it is given, in terms of the Bessel function of imaginary argument $I_0(z)$, by Rice's distribution (see Whalen 1971 and Rice 1958):

$$P_h(x) = e^{-x} e^{-|c|^2} I_0(2|c|\sqrt{x}). \quad (27)$$

It is properly normalized to unity. For the whole set

$$\begin{aligned} p_h(x_i) &= \frac{1}{N} \sum_j P_h(x_j) \prod_{k \neq j} P_0(x_k) = \\ &= \frac{1}{N} \sum_j \exp \left(-\sum_i x_i - c^2 \right) I_0(2|c|\sqrt{x_j}). \quad (28) \end{aligned}$$

j labels the spectral point where the signal is found, assumed to lie with equal a priori probability in the observed spectral range. Note that in doing so we neglect the fact that, at a given amplitude and for given masses, the distance of the source increases with the frequency (eq. (IS)); thus the a priori probability of a signal increases with the frequency.

We choose to declare 110 detection if no spectral component is larger than a new threshold \bar{x}' , function of the amplitude and determined by the false dismissal probability

$$\begin{aligned} \int_{C_{\bar{x}'}} d^N x p_h(x_i) &= \alpha(\bar{x}', |c|) = \\ &= (1 - e^{-\bar{x}'})^{N-1} \int_0^{\bar{x}'} dx P_h(x). \quad (29) \end{aligned}$$

This corresponds to the probability of a signal being present only in the bin with largest amplitude.

In practice, for a given record, and after having carefully eliminated all the spurious spectral components which can be ascribed to other causes and therefore are not random, we set \bar{x}' equal to x_m , the largest of the x_k 's and declare, at the level of confidence $1 - \alpha$, *no detection*, if the normalized amplitude is smaller than the threshold $|c(\bar{x}')|$ given by the previous equation. The function

$$\int_{\bar{x}'}^{\infty} dx P_h(x) = Q(\sqrt{2}|c|, \sqrt{2}\bar{x}')$$

can be written in terms of *Marcum Q-function*

$$Q(u, v) = 1 - \int_0^v dw w \exp \left[-\left(\frac{w^2 + u^2}{2} \right) \right] I_0(uw), \quad (30)$$

which has been extensively studied (Whalen 1971, Sec. 4.4).

If then $u \approx |c|\sqrt{2}$ and $v \approx \sqrt{2}\bar{x}' \gg 1$, $|u - v| \ll |u|$, using the asymptotic expression for the Bessel function, we see that most mass of the integrand lies near u , so that $1 - Q \ll 1$ and

$$\alpha = (1 - Q)(1 - Ne^{-\bar{x}'} + \dots) \approx 1 - Q + \dots, \quad (31)$$

almost independent of N . The danger of false dismissal mainly comes from the bin with largest amplitude.

In this case it is convenient to map the probability α into the normal gaussian variable s :

$$\alpha(\bar{x}', |c|) = \frac{1}{\sqrt{2\pi}} \int_{-\infty}^s ds' \exp(-s'^2/2).$$

For instance, when $\alpha = 0.1$, $s \approx -1.30$. In that limit we have the 'rule of thumb'

$$\sqrt{2}\bar{x}' \approx \sqrt{2}|c| + s; \quad (32)$$

in other words, the variable $\sqrt{2}\bar{x}'$ is normally distributed around the mean $\sqrt{2}|c|$. When $\bar{x}' \approx 13.38$ this gives $|c| = 4.58$. In both options we have chosen a simple and practical class of partitions of X i.e., N -dimensional cubes. However, this partition does not quite fulfill Neyman-Pearson criterion, which requires also to minimize the risk of false dismissal (in option A) and of false detection (in option B); in principle one should consider general partitions. Formally, in option A) let $X = X_0 \cup X_1$, where X_1 is the 'detection' set, with

$$\int_{X_1} d^N x p_0(x_k) = \alpha; \quad (33)$$

in option B), for a given signal level c , let $X = X'_0 \cup X'_1$ where X'_0 is the 'no detection' set, with

$$\int_{X'_0} d^N x p_h(x_k) = \alpha. \quad (34)$$

A way to construct these partitions is provided by the Neyman-Pearson theorem. Considering first option A), we construct, for all positive numbers k , the class of sets

$$X_k = \{x_k : \frac{p_h(x_k)}{p_0(x_k)} > k\} \quad (35)$$

The appropriate value of k is determined by eq. (33).

In our case the Neyman-Pearson surface

$$\begin{aligned} \frac{p_h(x_k)}{p_0(x_k)} &= \frac{1}{N} \sum_j \exp(-c^2) I_0(2|c|\sqrt{x_j}) \\ &\propto \sum_j I_0(2|c|\sqrt{x_j}) \approx k' \end{aligned} \quad (36)$$

is of interest far from the origin, corresponding to large thresholds; also, $|c| \gg 1$. The function $I_0(2|c|\sqrt{x})$, for large values of the argument, increases exponentially with \sqrt{x} ; hence we expect the summation in the previous equation to be dominated by the largest coordinate x_m and be approximated by:

$$k' \approx I_0(2|c|\sqrt{x_m}). \quad (37)$$

Since the Bessel function I_0 increases with its argument, hence with x_m , X_k consists of all points in X for which the largest coordinate is greater than some value x_m determined by k (and α). The complement X_k of this set is just the cube of size x_m . Our choice of the 'no detection set' does not quite minimize the false dismissal probability and will give a threshold somewhat higher than necessary.

4. The data set

As explained in (Bertotti et al. 1992), the data have been obtained using open and closed loop receiving systems at the DSN station and Digital Tone Extractors (DTE) at the VLBI antennas. The three different types of data have been preprocessed and reduced to data sets with the same structure and content (the sky frequency of the received radio signal with ancillary information).

The output of open loop receivers is essentially a time sequence of voltage samples of the down converted carrier signal. The measurement bandwidth can be selected according to the signal slew rate and SNR. For the ULYSSES experiment, where the frequency drift is low and the only relevant information resides in the main carrier signal, the bandwidth was chosen to the smallest available value (100 Hz, corresponding to a sampling rate of 200 Hz). In spite of the low sampling rate, about 6 Gb of open loop data have been collected during the 28 days of the experiment. The reconstruction of the sky frequency was performed with a digital phase lock loop programmed at an integration time of 1 sec. Due to their superior quality, especially at high frequencies, open loop data are the primary data set of the experiment.

Closed loop receivers are routinely employed by the DSN for spacecraft tracking and radiometric measurements. These data have been used as a back-up whenever open loop data were not available, provided that the time sequence had no appreciable degradation.

The Digital Tone Extractor (DTE), built by G. Co moretto, has been designed to measure the phase and the amplitude of a coherent signal at the output of a MARK 111 VLBI receiver. The digital data stream from the MARK 111 is correlated with a sine and a cosine waveform generated by the JI- maser at a frequency programmed by a control computer. The output of both mixers is then low-passed through an integrator to reconstruct the phase and the amplitude of the received signal. The whole system acts as a fully programmable, real-time phase-locked loop. With the flexibility of an open loop system, the DTE has the advantage of much less requirements for data storage.

Once the sky frequency have been reconstructed from the recorded data, a careful procedure has been used to edit the outliers, eliminate (as far as possible!) the ordinary Doppler effect and the contribution of the intervening media (Bertotti et al. 1992, Agresti et al. 1986). The orbital Doppler shift can be removed either using the Orbit Determination Program developed at Jet Propulsion Laboratory (Moyer 1971) or by fitting the data to a linear combination of the six functions

$$1, t, \sin\omega_E t, \cos\omega_E t, t \sin\omega_E t, t \cos\omega_E t,$$

where ω_E is the angular velocity of the Earth (Cerkendall and McReynolds 1969). In a later paper we shall discuss also the noise structure and compare the two methods; in

the present paper we confine ourselves to the much simpler six parameter fit. Note also that the separation between the orbital contribution and the gravitational signal, at least a billion times smaller, is possible because the former has a main part at the time scale of 1 y and a line at the frequency ω_E .

The second largest contribution to the frequency shift (although a million times smaller, 20 to 40 mHz) comes from the time-varying, elevation-dependent optical path in the troposphere. Several models may be employed to calibrate or fit out this effect. We have used a deterministic calibration which combines meteorological data measured at the tracking sites with a simple geometrical model due to Black and Fisher (1984). The random fluctuations of the tropospheric refractive index are believed to be negligible at the sensitivities of the present experiment and have never been clearly detected in our data.

The ionosphere produces similar, although more complex, contributions. The ionospheric path delay varies not only with the elevation, but also as a consequence of day-night changes of the plasma density. Although it is possible to filter out this contribution with a polynomial fit, it is far more reliable to exploit the dispersive properties of the ionosphere and estimate the path delay variations from dual frequency or Faraday rotation measurements. The DSN routinely provides, for each passage, a polynomial interpolation of the expected path delay along the line of sight to the spacecraft. Since the raw ionospheric data are obtained with spacecraft in different parts of the sky, a model of the ionosphere is used. The degree of the interpolating polynomials is in general low (4 or 5) and, therefore, the data can compensate only for long time scale variations (short 2 h). As for the troposphere, random ionospheric fluctuations should produce a negligible effect and may be partially compensated for in a statistical way with the Wiener Filter described below.

The interplanetary plasma is likely to be the dominant noise source in the ULYSSES experiment and therefore a special effort has been devoted to its reduction. We have applied a statistical compensation procedure based on a Wiener optimum filter (Bertotti et al. 1993; see also Savitch 1973). The filter estimates the up-link plasma contribution near opposition from the down-link contribution, obtained as a linear combination of the S and X band observable quantities:

$$y^* = \frac{f_S^2 y_S - f_X^2 y_X}{f_S^2 - f_X^2} \quad (38)$$

The employed Wiener filter is also nearly optimal for the random noise due to the ionosphere, which is therefore reduced. An overall reduction of the Allan deviation of about 30% of the Allan deviation has been obtained at long time scales (500 to 1000 sec).

We have considered only a time sequence of 14 days (see Fig.1) and based our analysis on the S- and the X-band phases of:

the DSN data for 6770 of the total time; the VLBI data for 63% of the total time.

The S-band was always noisier than the X-band. The VLBI data are always available in conjunction with simultaneous DSN data. Each record consists in a sequence of numbers $y(t_i)$, with sampling time Δt . Of 1 sec for the DSN record, 0.4 and 0.25 sec for the DTE at Medicina and Kashima, respectively. Although the tracking has been continuous from all DSN complexes, it has been impossible to use open loop receivers at the Deep Space Station (DSS) 12 at Goldstone, which were scheduled to start operating on day 64. Because of their larger noise at high frequencies, in general we have not used closed loop data; the gaps in the DSN data are mostly due to this reason and not to poorer performance. The data have been omitted when a poor stability could be traced to hardware malfunction, spacecraft manoeuvres or bad weather. Since there was no coverage in correspondence to the Goldstone passages, the VLBI sequence shows gaps of about 8 hours every day, so that the two time sequences (DSN and VLBI) almost overlap. Also we did not include data acquired at elevations below 15° for reception at a different station (three way) and 20° for reception at the same station (two way). The removal of the orbital Doppler shift in short three way passages has been done with the Orbit Determination Program.

Unfortunately the spectra are corrupted by the rotation of the spacecraft, with nominal frequency $1/12$ Hz, and its variation; this produces directly or, through aliasing, indirectly, many strong lines above $f_2 = 5 \cdot 10^{-2}$ Hz. It is interesting to note that the analysis of these lines provides accurate information on the attitude of the spacecraft and its rotational motion (less and Arduini 1994). We have confined our analysis to the band between $f_1 = 2.3 \cdot 10^{-4}$ Hz $\approx 1/T_1$ and f_2 , including about

$$N = f_2 T_1 = 65,000$$

spectral bins of width $1/T_1 = 8.3 \cdot 10^{-7}$ Hz.

What is the best frequency resolution attainable with a discrete Fourier transform, one wonders if, for the only sake of determining whether a line is present, a coarser spectrum provides a better alternative. The answer is not obvious: while the averaging depresses the signal, by diminishing the number of degrees of freedom of the noise, it also impairs its possibility of simulating large spectral lines. With an analysis of the false alarm probability on an averaged spectrum we have confirmed that this is not the case.

5. Threshold for periodic signals

Fig. 2 confirms the expectation that the spectral amplitudes have a gaussian distribution, except for two outlying lines. In the observed distribution of occurrences of the DSN time sequence the lines that lie above the threshold

$\bar{x} = 13.38$, corresponding to $\alpha = 0.1$, or 90% confidence level, occur at the following frequencies and normalized amplitudes

$$\begin{aligned} 1. & 1.66590 \cdot 10^{-2} \text{ Hz}, & 16.1; \\ 2. & 3.3333910 \cdot 2117 & 13.5; \end{aligned}$$

The expected number of occurrences $N e^{-\bar{x}}$ in a sample of 65,000 bins is, respectively, 6.610^{-3} and 8.910^{-2} . They deserve attention as candidate signals.

However, none of these lines can be attributed to gravitational waves and detection (option A) is not attained. Indeed, the VLBI time sequence does not show any outlier of this magnitude and any coincident power enhancement; indeed, the normalized amplitudes at these frequencies in the VLBI power spectrum are 1.1 and 3.8. The nature of these lines is not yet fully understood. A possible explanation, that needs however further investigation, could be the aliasing of strong high frequency lines due to the rotational dynamics of the spacecraft. Since the final Nyquist frequency for the DSN record was lower than for the VLBI data (the sampling time Δt was set at 0.25 sec at Kashima, 0.4 sec at Medicina and 1 sec for the DSN open loop measurements), all rotational lines that lie between 0.5 and 1.25 Hz are aliased only into the Nyquist band of the DSN measurements, while are correctly filtered out in the DTE data processing. However, one cannot exclude an instrumental origin.

Following option B, we then look for upper limits to the signal amplitude. The simpler way to estimate the maximum amplitude of a signal hidden in the noise is to consider the 1σ detection level, i.e. to measure, for each frequency, the spectral level corresponding to a normalized amplitude $\bar{x} = 1$. Such a line would give rise to a false alarm with probability $1/e = 0.37$ and, therefore, about 37% of the lines would appear at a higher level. This level corresponds roughly to a signal with the same magnitude as the noise ($\text{SNR} = 1$). The one-sided power spectral amplitude is related to the dimensionless amplitude h of a sinusoidal gravitational wave through the relation (see eq. (5) for the definition of F)

$$h(f) = \frac{1}{|F(fT_1, \theta)|} \sqrt{\frac{2S_y(f)}{T_1}} \quad (39)$$

This quantity is plotted in Fig. 3 for the DSN (lower curve) and the VLBI data (upper curve), with the generic value 1 for the (unknown) instrumental factor $|F|$. As expected, the sensitivity of the VLBI data is worse at high frequencies, due to the smaller size of the antennas and larger thermal noise. One may conclude that, using the smoothed spectrum as a figure of merit, the sensitivity of the ULYSSES experiment varies from about $3 \cdot 10^{-15}$ at low frequencies to 10^{-15} at high frequencies. The experimental curve can be fitted with

$$h(f) \approx 310^{-16} (f/\text{Hz})^{-0.26}. \quad (40)$$

However, the analysis of Sec. 3 and eq. (32) in particular, shows that signals up to about 4.6 times this level can be hidden in the data record, without giving rise to detection, at the 90% confidence level.

Fig. 2. The histogram of the dimensionless spectrum (eq. (20)) confirms its gaussian character. Squares and plus signs refer respectively to the DSN and VLBI time sequences. The outlying points are discussed in the text.

Fig. 3. Equivalent dimensionless amplitude of the gravitational waves obtained from the DSN (solid line) and VLBI (dashed line) time sequence. The spikes in the DSN data are discussed in the text.

G. Chirped signals

We confine ourselves to linear chirps (eqs. (14) and (15)), a simple generalization of strictly periodic signals which is free from any assumption about the prevailing energy loss (or gain!) of the binary system. (However, we have implicitly assumed an almost circular orbit; note that the dynamical friction with the background may increase the eccentricity (Ebisuzaki et al. 1991; Fukushige et al. 1992; Vecchio et al. 1994).)

The method, as developed by Tinto and Armstrong (1989), consists in multiplying the record $y(t)$ by $G(t) = \exp(-\pi i \beta t^2)$ - which changes each frequency at the rate β - and considering the spectrum of the product $y_c(t, \beta) = y(t) G(t)$. The allowed range of β is determined by the requirement that the (positive) frequency stays within the band (f_1, f_2) ; denoting with f the frequency in the middle of the record, this means:

$$-2(f - f_1) < T_1 \beta < 2(f_2 - f). \quad (41)$$

The frequency resolution $1/T_1$ sets the best possible resolution $2/T_1^2$ for β ; this gives in the $(f, T_1 \beta)$ plane a total of

$$N_c = (f_2 - f_1)^2 T_1^2 \approx f_2^2 T_1^2 \approx N^2$$

available points.

Physical arguments restrict the relevant domain further. β should be positive, corresponding to an energy loss. If the loss is due to gravitational waves, another constraint comes from the neglect of any acceleration in frequency; to wit, the frequency change between the middle and the end points of the observation run must be less than the frequency resolution $1/T_1$:

$$T_1^3 |\dot{\beta}| < 8.$$

Since the frequency changes like $1/(t_0 t)^{3/8}$, the *braking index* (well known in the theory of pulsars) is

$$\frac{\dot{\beta} f}{\beta^2} = \frac{11}{3} \quad (42)$$

and hence, as also noticed by Tinto and Armstrong 1991,

$$T_1^3 \frac{\beta^2}{f} < \frac{24}{11}. \quad (43)$$

Numerically this reads

$$\beta < 1.1 \cdot 10^{-9} \sqrt{f} \text{ sec Hz}^2. \quad (43')$$

A lower limit would be obtained analyzing together two runs separated in time.

The relevant domain is divided in two frequency ranges by the frequency f^* , where

$$2T_1(f_2 - f^*) = \sqrt{\frac{24}{11}} f^* T_1$$

Since $T_1 f_2 \gg 1$ we obtain

$$f^* = f_2 - \sqrt{\frac{6 f_2}{11 T_1}},$$

not very different from f_2 . We can now evaluate the total number N'_c of relevant points in the $(f, T_1 \beta)$ plane at the maximum resolution. The first interval prevails and gives

$$N'_c \approx \frac{2}{3} \sqrt{\frac{6}{11}} (T_1 f_2)^{3/2} \approx 8 \cdot 10^6 \quad (44)$$

If the chirp is caused by gravitational waves, the de-modulation of the signal should produce three lines in the power spectrum, at frequencies

$$f, \quad f - \beta \frac{1 + \cos \theta}{2} T_1, \quad f - \beta T_1$$

(Tinto and Armstrong 1991). These lines can be resolved only if $\beta T_1^2 > 1$; since the rate is limited by (43), this is impossible if

$$2 \int_{-11}^{6N} \frac{T}{T_1} < 1 \quad (45)$$

In our case this number is **0.4**.

The multiplication by $G(t)$, of course, does not change the gaussian character of the variable; moreover, since $|G(t)|$ is constant, $y_c(t, \beta)$ is obviously white if so is $y(t) = y_c(t, 0)$. (However, in the non linear regime the change in amplitude will add colour to the spectra.) Hence the normalized spectra of the noise, $x_{c,k}(\beta) = |y_{c,k}(\beta)|^2$, for a given β , are still uncorrelated and exponentially distributed according to eq. (24); but the amplitudes for different β 's are correlated.

For a simpler formalism we take the quantity $y_c(t, \beta)$ (and, of course, $y(t)$) already (in the average) whitened and normalized; then in the average

$$\langle y_c^*(t) y(t') \rangle = T_1 \delta(t - t')$$

and, for the complex spectral amplitudes

$$y_k = \frac{1}{T_1} \int_{T_1/2}^{T_1/2} dt y(t) \exp(-2\pi i f_k t),$$

$$\langle y_k^* y_h \rangle = \delta_{kh} \langle x_k \rangle = \delta_{hk}$$

For the chirped variables

$$\langle y_c^*(t, \beta) y_c(t', \beta') \rangle = T_1 \delta(t - t') \exp[-i\pi(\beta - \beta')t^2] \quad (46)$$

and, taking the Fourier transform

$$C(\Delta f, \Delta \beta) = \langle y_{c,k}^*(\beta) y_{c,h}(\beta') \rangle = \frac{1}{T_1} \int_{T_1/2}^{T_1/2} dt \exp[-2\pi t \Delta f - i\pi t^2 \Delta \beta], \quad (47)$$

with

$$\Delta f = f_k - f_h, \quad \Delta \beta = \beta - \beta',$$

This is the required correlation function for the spectral amplitudes in the $(j, T_1 \beta)$ plane, with the correct behaviour when $\Delta \beta = 0$. It is normalized to $C(0, 0) = 1$; elsewhere $|C(\Delta j, \Delta \beta)| < 1$. This correlation function determines the (gaussian) probability distribution $w(y_c)$ for the noise in the space of the complex amplitudes $Y = \{y_{c,k}(\beta)\}$.

We look for the value of β - call it $\hat{\beta}$ - which makes $\max_k \{x_{c,k}(\beta)\}$ largest and take it as the candidate for the 'true' chirping rate. The data space Y has now a much greater number $2N_c$ of dimensions than before; the noise has a greater chance of simulating the signal and we expect a higher threshold \hat{x}_c for false alarm. The rigorous answer to this question entails integrating $w(y_c)$ over a N_c -dimensional cube, a seemingly impossible task; we use instead a heuristic method.

The total number of effectively independent modes $N_{c,\text{eff}} = N N_{\beta,\text{eff}}$ is the product of number N of frequency bins and the number $N_{\beta,\text{eff}}$ of the effectively independent modes for the rate, or the number of independent intervals in rate: $C(0, \beta_2 - \beta_1)$ is small if β_1 and β_2 lie in different intervals. This number has also a practical importance: it gives the largest spacing in the rate

$$\Delta_m \beta = \frac{2f_2}{T_1 N_{\beta,\text{eff}}}$$

we need for a reliable numerical calculation. This suggests that $N_{c,\text{eff}} = N N_{\beta,\text{eff}}$ is related also to the stability of the numerical calculation of the largest amplitude.

Both questions can be addressed with numerical simulations. We have generated a large number K of realizations of a gaussian, uncorrelated time sequence $y(t)$ and, for each of them and for all the available values of the rate, constructed the coordinates $|y_{c,k}(\beta)|^2 = x_{c,k}(\beta)$ of the corresponding point β in the space Y and evaluated their maximum x_m for each spacing

$$\Delta \beta = \frac{2f_2}{T_1 N_{\beta,\text{eff}}}$$

When $N_{\beta,\text{eff}}$ increases we expect first the average $\langle x_m \rangle$ over different realizations to increase proportionally to $\ln N_{\beta,\text{eff}}$ (see eq. (26)); when the correlation between neighbouring values of β is significant, $\langle x_m \rangle$ should reach an asymptotic value. The numerical simulations confirm this. The curves are flat, when $N_{\beta,\text{eff}} \approx N$, corresponding to $\Delta \beta = 2/T_1^2$. $N_{\beta,\text{eff}}$ can be estimated as the abscissa of the knee in the curve (see Fig. 4). Of course the position of the knee and $N_{\beta,\text{eff}}$ depend on the length of the test sequences; we estimate

$$N_{\beta,\text{eff}} \approx 0.3 N. \quad (48)$$

in the first interval we expect (eq. (26)) $\langle x_m \rangle = \ln N + \ln N_{\beta,\text{eff}}$; indeed the three curves in Fig. 4 differ by $\approx 3\%$.

For each spacing in Y we have also counted the number $K(\hat{x})$ of times the point \hat{x} lies outside a cube of side \hat{x} . The false alarm probability is then

$$\alpha = \frac{K(\hat{x})}{K} \quad (49)$$

We can relate the two simulations as follows. Eq. (24), which refers to independent spectral amplitudes, provides

their number N in terms of α and \bar{x} ; we use the same expression to define, in general]

$$N'_{\text{eff}} = \frac{\ln(1 - \alpha)}{\ln[1 - \exp(-\bar{x})]}. \quad (50)$$

As the threshold \bar{x} increases, we expect that this number tends an asymptotic value, which we take to measure the effective number of degrees of freedom of our correlated gaussian variables. This expectation is indeed confirmed (Fig. 5) and the asymptotic value is about 0.3 N , in agreement with the previous estimate. From Fig. 5 we also see that the ratio N'_{eff}/N^2 is roughly independent on the length N of the test sequences.

Fig. 4. The effect of the change in rate resolution $\Delta\beta \propto 1/N_\beta$ on the largest mean amplitude $\langle x_m \rangle$ (given in the ordinate) in a numerical simulation; the knee corresponds to the effective number of degrees of freedom in the rate. The three curves show also the effect of varying the number N of data points used in the simulations from 2048 (upper curve) to 1024 and 512 (lower curves).

If a gravitational wave signal

$$h \exp(2\pi f_t t + i\pi\beta_t t^2)$$

is present at the (unknown) ‘true’ frequency f_t and ‘true’ rate β_t , it generates in the appropriate $(f, \beta T_1)$ region the response

$$hC(f - f_t, \beta - \beta_t),$$

generally different from zero (except for $\beta = \beta_t$ and $f \neq f_t$). This is the signal we must look for. In Appendix B we study the shape of this response; in Appendix A we show, according the Neyman Pearson theorem, that $x_m = \max_\beta \{\max_k \{x_{c,k}(\beta)\}\}$ is indeed the correct variable to compare with a threshold.

We have analyzed the DSN and VLBI time sequences with this method. Figure 7 shows the two histograms

Fig. 5. The result of a numerical simulation to evaluate the effect of the chirping variability on the false alarm probability: in the ordinate we plot $N'_{\beta, \text{eff}}/N$ (eq. (50)), which gives the fraction of the independent values of β , as a function of the threshold.

of the probability density function for the dimensionless amplitude x ; each of them has been obtained by combining the different histograms obtained for different (positive) values of the rate β . About $N_\beta = 700$ different, equally spaced values of β have been used, from $\beta_1 = 3.29 \cdot 10^{-13} \text{ Hz}^{-2} = 1/(2T_1^2)$ to $\beta_2 = 2.40 \cdot 10^{-10} \text{ Hz}^{-2}$. The upper limit is given by the linearity condition (43). The smoothing frequency interval for the computation of the normalized amplitude (eq. 20) was chosen equal to 2.10^4 Hz , i.e. $N = 246$.

In this domain the DSN sequence has the largest value of x is 18.91, at $\beta = 1.38 \cdot 10^{-11} \text{ Hz}^2 = 1.19 \mu\text{Hz}/\text{d}$ and the frequency (in the middle of the record) $1.9985 \cdot 10^9 \text{ Hz}$. Unfortunately the frequency rate is too low to resolve the triplet of lines predicted by the theory (eq. 45). In a data set with about $N_{c,\text{eff}} = 0.3 \times 700 \times 65,000 = 1.36510^7$ degrees of freedom the occurrence probability of this line is $8.36 \cdot 10^{-2}$; the factor 0.3 has been obtained with the numerical simulations (eq. (48)). The probability for the second largest line, at $x = 18.40$, is 0.14, below our 10% threshold for false alarm. The statistical significance of the chirp at $x = 18.91$ is enhanced by the VLBI sequence; indeed, at that frequency and rate we find a line with $x = 11.39$, with a probability $1.1 \cdot 10^{-5}$. Although the two sequences are partially correlated, it is unlikely that this line is due to chance.

A more careful analysis shows, however, that the chirp is probably due to instrumental effects. We have generated six subsets of the DSN and VLBI time sequences. In each of them all the data related to one of the three DSN complexes have been substituted by zeros. It turns out that the chirp disappears only in the time sequences (DSN and VLBI) in which the contributions from the Madrid com-

plex have been edited out; indeed, at the suspect frequency and rate we find normalized amplitudes of 2.32 and 1.19. No significant enhancement was found for adjacent values.

On the basis of these results one may exclude a gravitational signature of the signal. A similar instrumental chirp was found in previous experiments (Anderson et al. 1993), although related to the Goldstone complex and with a much larger frequency drift. It would be important for future experiments and interesting in itself to trace their origin.



Fig. 6. Histogram of the dimensionless spectrum for the linearly chirped case, for the DSN and the VLB time sequences. The two lines at $x > 18$ are found in the DSN data and discussed in the text.

7. Conclusions

It is interesting to apply these results to the galactic centre, where, at $r \approx 10^4$ pc $\approx 10^{12}$ sec, a massive black hole of mass up to $\approx 2 \cdot 10^6 M_\odot$ is likely to sit (Genzel & Townes 1987, Blitz 1993 and other papers). Note that our detector had a favourable orientation ($O \approx 1090$). In this sect. [1] we use as units Hz and Hz^2 for the frequency and the rate, respectively. From eq. (8), the expected amplitude from a binary system with a period $2/f$ at the galactic centre looks encouraging:

$$h \approx 8.7 \cdot 10^{-13} \left(\frac{m}{10^6 M_\odot} \right)^{5/3} (f \text{ Hz})^{2/3}, \quad (51)$$

however, the data are significant only in a very small region in the (f, β) plane.

In the linear chirp regime, irrespective of the masses, the time to coalescence is determined by the frequency anti the rate:

$$t_0 - t \approx \frac{3f}{8\beta}; \quad (52)$$

hence (eq. (10)) the amplitude is given by

$$h \approx \frac{8\beta}{3A\pi f^3} = 6.2 \cdot 10^{-15} \frac{\beta}{f^3}. \quad (53)$$

At $\text{SNR} = 1$ a source cannot produce a line stronger than our measured amplitudes $h(f) = \sqrt{2S_y(f)/T_1}$. Since our data, even in the chirped case, are well represented by eq. (40), namely,

$$h(f) \approx 3 \cdot 10^{-16} f^{-1/4}, \quad (40')$$

they are relevant only in the region

$$21\beta > f^{11/4}. \quad (54)$$

Fig. 7. The relevant regions of the (f, β) plane. Data are available below the upper curve (and in the symmetrical region for negative rate). For a source in the galactic centre the condition $\text{SNR} = 1$ can be fulfilled only above the line b ; the linearity condition (43') restricts the data below the line a .

On the other hand the linearity condition (43') places an upper bound to the rate and restricts the region to a very small triangle near the lower cut off $f_1 = 2.3 \cdot 10^{-4}$ Hz. At this cut off the significant interval for the rate is

$$4.7 \cdot 10^{-12} < \beta < 1.6 \cdot 10^{-11};$$

the lower bound (54) grows faster than the upper bound (43') and meets it at the frequency $j' \approx 410 \cdot 4$, less than twice j_r . Only in this region (at $\text{SNR} \approx 1$) we are allowed to constrain the mass parameter with eq. (51), namely

$$m < (h \cdot 10^{15})^{3/5} (1000f)^{-2/5} 17,000 M_\odot, \quad (55)$$

At the lowest frequency f_1 this limit for m is about $60,000 M_\odot$. If one of the two masses, $M_1 = p$, is much smaller than M , from eqs. (7) and (55) we get

$$\mu = m^{5/3} M^{-2/3} < 5800 M_\odot. \quad (56)$$

The time to coalescence, of the order of a few years, is so low that such a hypothetical source does not have much astrophysical value. At the orbital period $2/j$, the semi major axis is less than 1 AU. This result was not

known when the report less (1994) was written. A search in ULYSSES data for non linear chirps (case 3. of Sec. 2) will extend the analysis above the line b . We expect that, at SNR = 1, a similar bound for the mass parameter will be obtained; however, a for a given level of confidence, the enlargement of the region in the (f, β) plane will increase the threshold.

A few general remarks are in order. The precise theoretical description of the sources embeds in the gravitational wave data much information about the sources and, when a positive detection is attained, makes them a powerful tool of research; vice versa, however, if detection is not attained, it makes more difficult to place constraints on the possible sources. The assumption of linear chirps we have made should be waived; of course, however, this implies a shorter lifetime and more improbable sources. Also, the importance of attaining lower frequencies of observation cannot be stressed too much. The search for wave trains in ULYSSES data would be much more effective for sources nearer than the galactic centre (see Sec. 2), but we did not pursue this exotic path. Finally, as stressed in the pioneering paper by Braginsky and Thorne (1976), the Doppler method seems best suited for the search for wide band pulses; in a subsequent paper we shall present this analysis of ULYSSES' data, which should marginally reach the Virgo cluster.

This experiment marks noticeable advances in the Doppler search for low frequency gravitational waves; exploiting the long record and using several (up to four) observable quantities, remarkable progress has been made in the sensitivity and in understanding the noise structure. More importantly, while in previous papers on Doppler detection the main emphasis was in increasing the sensitivity, here, due to the large of spectral points available, we have been able to draw definite conclusions on the relevant astrophysical sources and, therefore, to assess the limitations of this technique.

From the instrumental point of view the main limitation of ULYSSES' experiment was the use of low frequency carriers, in particular in the up-link. This problem will be solved with the CASSINI mission (to be launched in December 1997) to Saturn, which will use X- and K_a-band in both links (Comoretto et al. 1992). In order to achieve still better performances in the mHz band, which could ensure successful detection according to conventional astrophysical expectations, a dedicated mission, using long baseline interferometers, is probably needed.

APPENDICES

A. Determination of the threshold for a chirped signal

As explained in Sec. 3, in order to minimize the false dismissal probability, we should construct in Y the 'detection

set' Y_1 , with

$$\int_{Y_1} dy_c w(y_c) \approx \alpha, \quad (\text{A.1})$$

in the following way: if $w_h(y)$ is the probability distribution of the observable quantities when a signal is present, among the surfaces

$$\frac{w_h(y)}{w(y)} = \text{const}, \quad (\text{A.2})$$

we choose the one which fulfills eq. (A.1). We show that, because of the relation between signal and correlation, this is essentially the same problem as in the case without chirp, eq. (36).

In order to concentrate on the mathematical structure, let the index $m = (f, \beta)$ stand for the coordinates in their appropriate ranges; taking $T_1 = 1$, f is an integer and β is an even integer. Accordingly, write C_{mn} (with $C_{nm} = 1$) for $C(\Delta f, \Delta \beta)$ and y_m for $y_{c,k}(\beta)$ (as in Sec. 6, the noise amplitudes are assumed to be white and normalized.) The 'true' point is $t = (f_t, \beta_t)$. The probability distribution for the noise is

$$w(y) \propto e^{-q},$$

where

$$q = \sum_{mn} y_m^* Q_{mn} y_n;$$

the hermitean matrix Q_{mn} ($= Q_{nm}^*$) is the reciprocal of the correlation matrix

$$\langle y_m^* y_n \rangle = C_{mn} = (Q^{-1})_{mn}. \quad (\text{A.3})$$

The response to a signal of complex amplitude h is just hC_{mt} , so that in that case $y_m - hC_{mt}$ is gaussian, with a probability distribution

$$w_h(y) \propto e^{-q_h};$$

here

$$q_h = \sum_{mn} (y_m - hC_{mt})^* Q_{mn} (y_n - hC_{nt}).$$

The fact that the response function is just the correlation matrix makes things simple and, because of eq. (A.3), leads to

$$q_h = q + h^* y_t - h y_t^* + |h|^2.$$

y_t is the observed amplitude at the 'true' frequency and rate. In computing the ratio (A.2) $\propto \exp(2|h||y_t| \cos \chi)$ we must now average over the (unknown!) relative phase of the wave χ and obtain, similarly as in Sec. 3,

$$\frac{w_h(y)}{w(y)} = \exp(-|h|^2) I_0(2|h||y_t|).$$

We see that the level surfaces, and hence the strategy of decision, depends only on the size of the largest spectral amplitude produced by the signal, $|y_t|$.

If both the frequency and the chirp rate have equal a priori probability, we must also average, with uniform

weight, the probability $w(y)$ over all values of t , obtaining the same equation (36) as before. With the same approximation we take the ‘detection set’ to be the complement of the cube in the space of the normalized spectra, with a side \bar{x} determined by the confidence level.

B. The correlation function for the chirped variables

We have estimated the correlation function of the chirped noise data

$$C(\Delta f, \Delta\beta) = \int_{-1/2}^{1/2} dt \exp(-\pi i \Delta\beta t^2 - 2\pi i \Delta f t). \quad (B.1)$$

If T_1 , the duration of the record, is the unit of time, f and $\beta/2$ are integers (generally very large) in the domain (41).

By completing the square in the exponent, this function can be evaluated in terms of Fresnel integrals $C(z)$ and $S(z)$, with

$$E(z) = C(2) + iS(z) = \int_0^z du \exp\left(i\frac{\pi}{2}u^2\right) \quad (B.2)$$

(Abramowitz & Stegun 1965). This is an odd function of the complex variable z , with the asymptotic expression

$$E(z) = \frac{1+i}{2} - \frac{i}{\pi z} \exp\left(i\frac{\pi}{2}z^2\right) + O\left(\frac{1}{z^3}\right). \quad (B.3)$$

We obtain:

$$C(\Delta f, \Delta\beta) \approx \exp\left(\pi i \frac{(\Delta f)^2}{\Delta\beta}\right) \frac{1}{\sqrt{-2\Delta\beta}} [E(u_+) + E(u_-)], \quad (B.4)$$

with the arguments

$$u_{\pm} = \sqrt{-\frac{\Delta\beta}{2}} \pm \Delta f \sqrt{-\frac{2}{\Delta\beta}}$$

When $\Delta\beta = 0$ we recover directly from eq.(B.2)

$$\begin{aligned} C(\Delta f, 0) &= 0 \quad \text{if } \Delta f \neq 0; \\ C(\Delta f, 0) &= 1 \quad \text{if } \Delta f = 0. \end{aligned}$$

Consider now the expression in the square bracket of eq.(B.4) in the general case, in which both arguments of the function $E(z)$ are large. There are two possibilities. If $|\Delta\beta| \gg |\Delta f|$ the two arguments are almost equal and the square bracket is almost $1+i$, twice the asymptotic value, yielding

$$C(\Delta f, \Delta\beta) \approx \frac{1+i}{\sqrt{-2\Delta\beta}} \exp\left(\pi i \frac{(\Delta f)^2}{\Delta\beta}\right), \quad (B.5)$$

with fractional corrections of order $\Delta f/(\Delta\beta)^{3/2}$.

Instead, if $|\Delta f| \gg |\Delta\beta|$, the two Fresnel exponentials almost cancel and the square bracket reads

$$E(z+\delta z) - E(z-\delta z) \approx$$

$$= -\frac{i}{\pi z} e^{i\pi z^2/2} \left[\left(1 - \frac{\delta z}{z} \right) e^{i\pi z \delta z} - 1 \right], \quad 3' - ' ' 2^1$$

with

$$z = \Delta f, \quad \frac{2}{\Delta\beta}, \quad \delta z = \sqrt{-\frac{\Delta\beta}{2}}.$$

Since $z\delta z = \Delta f$ is an integer,

$$e^{i\pi z \delta z} - e^{-i\pi z \delta z} = 2i \sin(\pi \Delta f) \approx 0$$

and

$$e^{i\pi z \delta z} + e^{-i\pi z \delta z} = 2 \cos(\pi \Delta f) \approx 2(-)^{\Delta f}$$

Therefore

$$E(z + \delta z) - E(z - \delta z) \approx (-)^{\Delta f} \frac{2i\delta z}{\pi z^2} \exp\left(i\frac{\pi}{2}z^2\right)$$

and hence, from eq.(B.4)

$$C(\Delta f, \Delta\beta) \approx -\frac{i\Delta\beta}{\pi(\Delta f)^2} (-)^{\Delta f}. \quad (B.6)$$

In both approximations the phase of the correlation function changes very rapidly from mode to mode.

Acknowledgements. This work is the result of the joint effort of many people, besides the team of the ULYSSES gravitational wave experiment; we are very grateful, in particular, to the Radio Science Support Team at JPL, to the staff of the Deep Space Network, to the ULYSSES project and to the staff of the Istituto di Radioastronomia (Bologna). The bulk of the data analysis was carried out by L. Iess; his work, until November 1, 1993 was supported by the Istituto di Fisica dello Spazio Interplanetario. We are also grateful to F. Tinti for his numerical work in the data analysis of the chirps.

LITERATURE

References

- Abramowitz, M., Stegun, I. 1965, *Handbook of Mathematical Functions*, Dover Publications, New York.
- Agresti R., Iess L., Bonifazi P. 1986 *Media calibrations of the Doppler signal for a gravitational wave experiment*, Internal Report IFSI-86-13.
- Anderson J.D., Armstrong J. W., Lau E.L. 1993, ApJ, 408, 287.
- Armstrong J.W. 1989, in: “Gravitational Wave Data Analysis”, B. F. Schutz ed., Kluwer, p. 153.
- Armstrong J. W., Estabrook F.B., Wahlquist H.H. 1987, ApJ 318, 536.
- Bertotti B., Ambrosini R., Asmar S.W. et al. 1992, A&A 292, 431.
- Bertotti B., Comoretto G., Iess L. 1993, A&A 269, 608.
- Bertotti B., Sivaram C. 1991 Nuovo Cim. 106 B, 1299.
- Black H.D. and Eisner A., 1984, J. Geophys. Res., 89, 2616.
- Blanchet and Sathyaprakash 1994, ‘Detecting the tail effect in gravitational-wave experiments’, Preprint.
- Blitz L., Binney J., Lo K.Y., Bally J. and Ho P. T. P. 1993 Nat 361, 417.
- Comoretto G., Iess L., Bertotti B. et al. 1990 Nuovo Cim. 13, 169,

- Comoretto G., Bertotti B., Iess L. and Ambrosini R. 1992
Nuovo Cim. 15C, 1193.
- Curkendall D. W., McReynolds S. R. 1969 J. Spacecraft and
Rockets 6, 520.
- Dhurandar S. V. and Sathyaprakash B. S. 1994 Phys. Rev.
D49, 1707.
- Ebisuzaki T., Makino I., Okomura S. 1991 Nat 354, 212.
- Fukushige T., Ebisuzaki T., Makino J. 1992 ApJ 396, L61.
- Genzel R., Townes C.H. 1987 ARA&A 25, 377.
- Iess L. 1994 Proc. of the X Conference of the Italian Society for
General Relativity and Gravitation, Bardonecchia. World
Scientific, p. .
- Iess L. and Arduini C. 1994 Attitude determination of Ulysses
spacecraft with precision Doppler tracking, To appear in:
Proc. 2nd ESA Conf. on Spacecraft Guidance, Navigation
and Control Systems, Noordwijk, April 12-15, 1994.
- Iess L., Bonifazi P., Bertotti B. and Comoretto G. 1987 Nuovo
Cim 10C 235.
- Kokkotas K., Królik A. and Tsegas G. 1993 'Statistical analy-
sis of the parameters of the gravitational wave signals from
a coalescing binaries' Preprint.
- Moyer T.D. 1971 Mathematical Formulation of the Double-
Precision Orbit Determination Program (DPODP) JPL
Technical Report 32-1257.
- Piran T., Stark J. F. 1986, in "Dynamical Spacetimes and
Numerical Relativity", J. M. Centrella ed. Cambridge Uni-
versity Press, p. 40.
- Rice S. 0.1958 Bell System Tech. J. 37, 581; reprinted in: 1954
Selected Papers 011 Noise and Stochastic Processes, ed. N.
Wax, Dover, p. 133.
- Sathyaprakash B. S. and Dhurandar S. V. 1991 Phys. Rev.
D44, 3819.
- Savich N. A. 1973 Radio Eng. and Electron Physics 18, 1004.
- Silvey S. D. 1970 Statistical Inference. Chapman and Hall.
- Thorne K. S. and Braginsky V. B. 1976 ApJ 204, L1.
- Tinto M., Armstrong J.W. 1991 ApJ, 545.
- Vecchio A., Colpi M. and Polnarev A. 1994. Orbital evolution
of a massive black hole pair by dynamical friction, to appear
in ApJ.
- Wahlquist H.D. 1987 Gen. Rel. Grav. 19, 1101.
- Whalen A.D. 1971. Detection of Signals in Noise. Academic
Press.

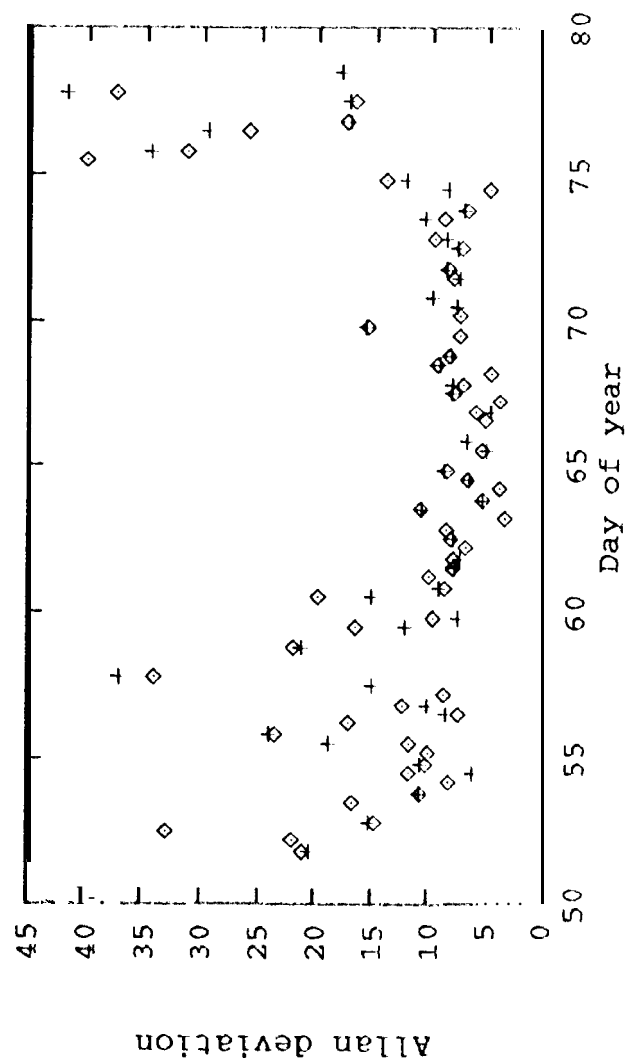


Fig. 1

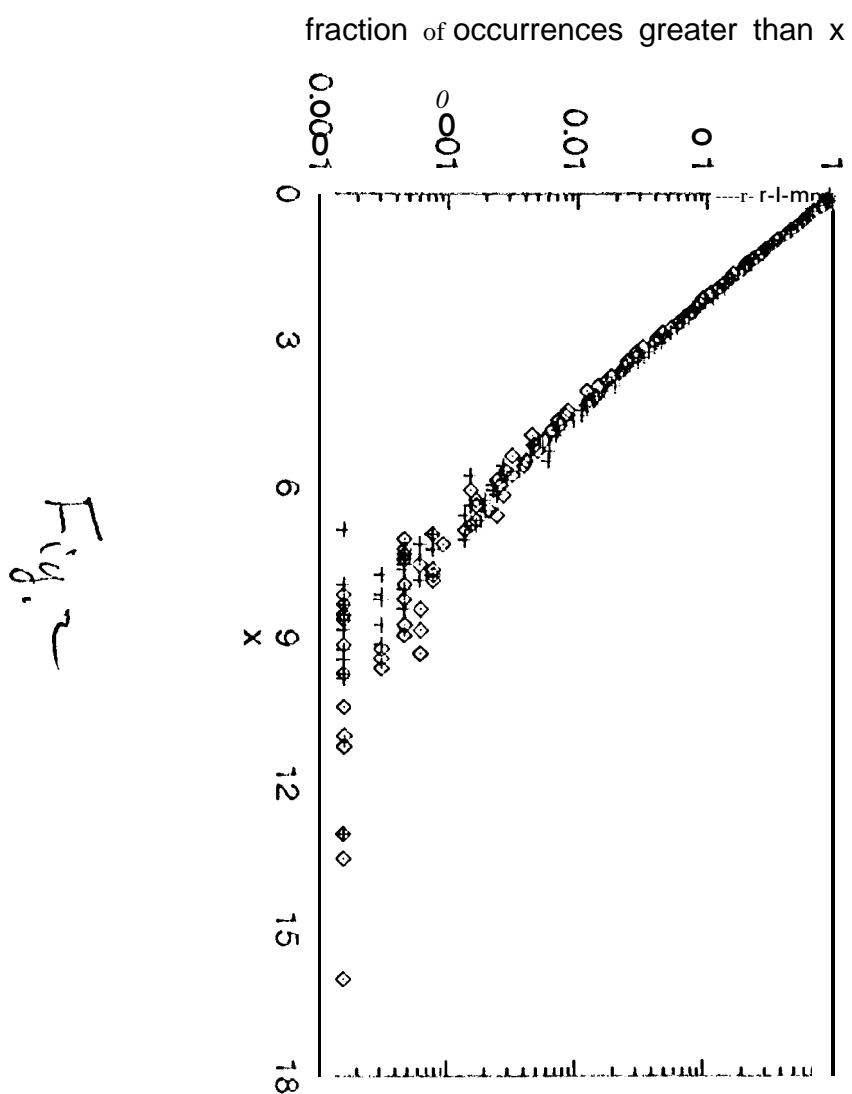


Fig.

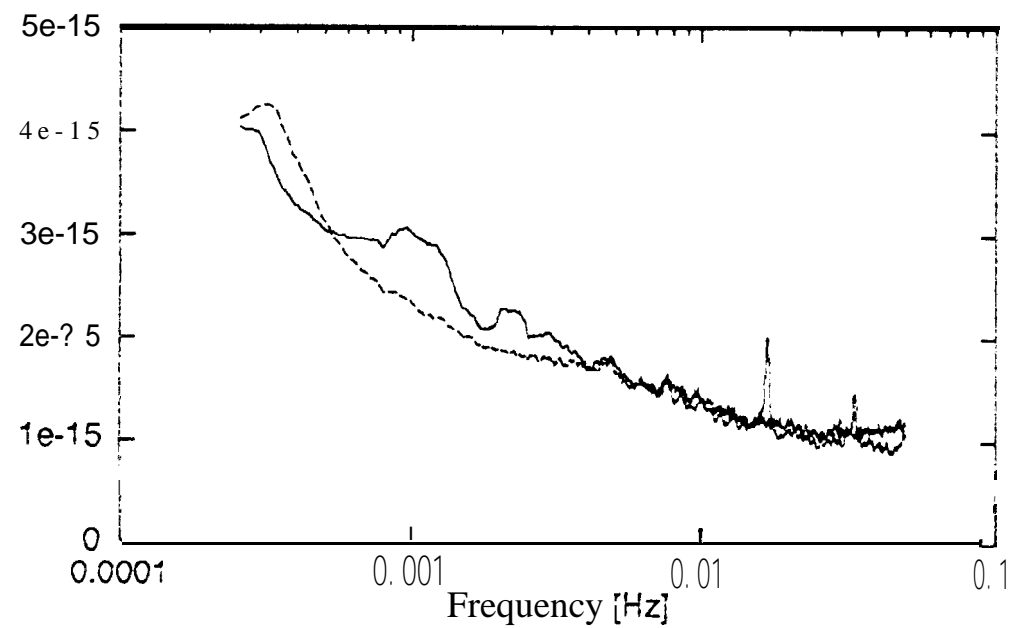


Fig. 3

-16.0, 25

Fig. 4

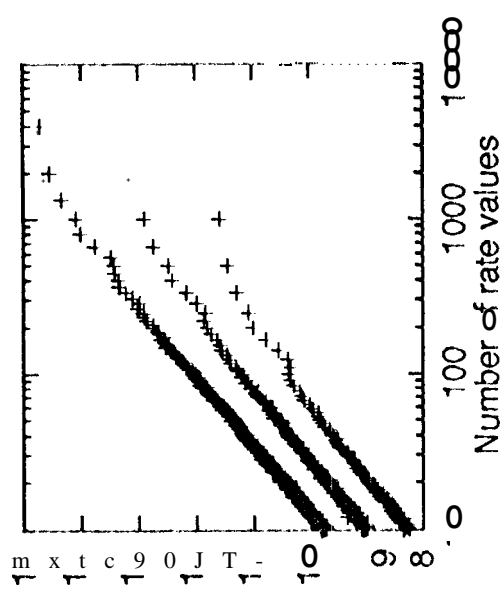
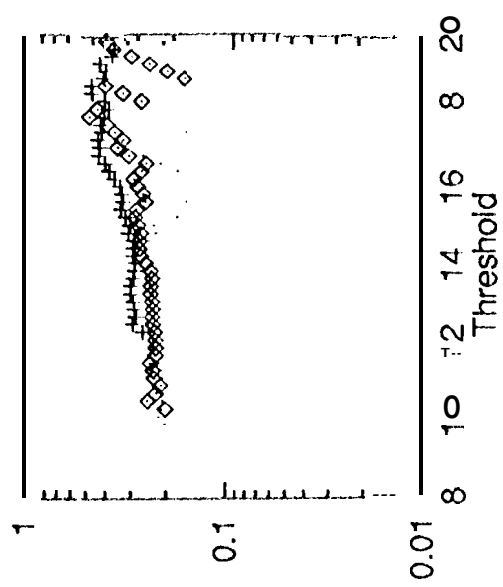


Fig. 5

Set 2, PC

Fig. 5



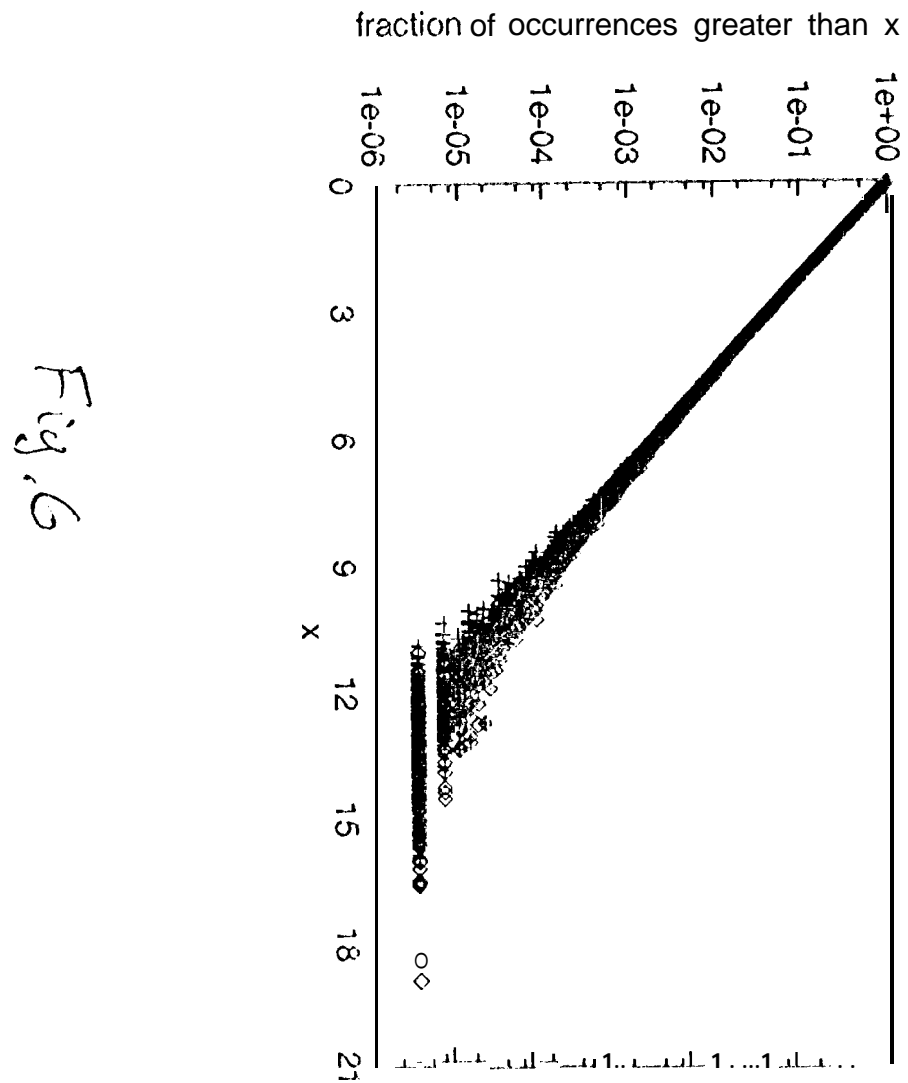


Fig. 6

-1
10⁻⁶
PS

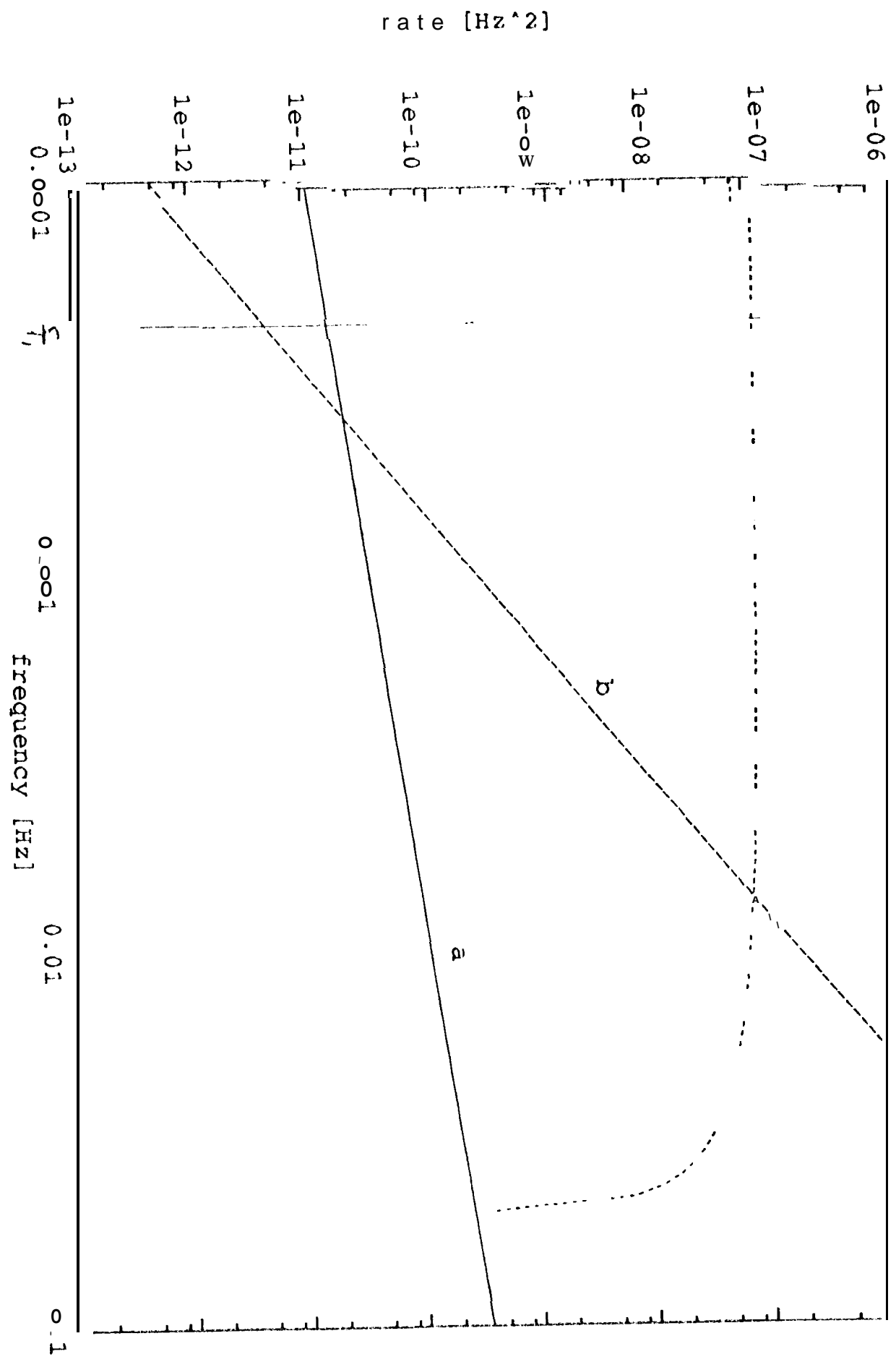


Fig. 7